L-42

# Analysis of Electromagnetic Scattering form Conducting Polygons by the Point Matching Method
## - Frequency Responses for Slight Variation of the Geometry -

* Shuichi Shinohara[1], Ryuichi Ohsawa[2], Shinichiro Ohnuki[3], Tsuneki Yamasaki [3]

Abstract: High precision analysis of electromagnetic scattering problems is performed for conducting cylinders with wedge cavities. We discuss the radar cross section for varying the normalized frequency and the direction of the specular reflection when the target has conducting plates which are parallel to the traveling direction of the incident wave.

## 1. Introduction

Analysis of electromagnetic scattering is important for target recognition and reduction of the RCS (radar cross section). The authors have proposed the PMM (point matching method) and reported that electromagnetic scattering problems can be analyzed with high accuracy [1] [2]. In this paper, we discuss the RCS for varying the normalized frequency and the direction of the specular reflection due to slight variation of the geometry.

## 2. Formulation

A scatterer shown in Figure 1 is assumed to be uniform along the *z*-axis. We impose the symmetry due to the *x*-axis on the scatterer. Hence, the incident wave is defined as follows;

$$H_z^{(i)}[p] = \frac{H_0}{2}\left\{\exp\left[jkr\cos(\theta-\phi_{in})\right] + (-1)^p \exp\left[jkr\cos(\theta+\phi_{in})\right]\right\},\ p=0,1. \quad (1)$$

Electromagnetic fields in all the separated regions are defined as follows;

$$H_z^{(S_l)} = \sum_{n=0}^{M_l-1} B_n^{(l)}[p] J_{\upsilon_l m}(kr_l)\cos(\upsilon_l m\theta_l) \quad (2)$$

$$H_z^{(S_l)} = \sum_{n=0}^{M_l-1} B_n^{(l)}[p] J_{\upsilon_l m}(kr_l)\cos(\upsilon_l m\theta_l),\ (l=1\sim 5) \quad (3)$$

where $\upsilon_l = \pi/\alpha_l$ , $\alpha_l$ is the edge angle at region $S_l$ , $p=0,1$ , $m=n\,(S_2\sim S_4)$ , $m=2n+p$ ( $S_1, S_5$ ).

The unknown expansion coefficients $A_n[p]$ and $B_n^l[p]$ are determined to satisfy the continuity conditions at the sampling points which are placed at the almost same interval on the boundaries [1].

## 3. Computational Results

Figure 2 shows the peaks of the RCS in the range of observation angles -40° to -65° when the angle of incidence $\phi_{in}=80°$. The value converges to the direction of the specular reflection when *ka* becomes large and the difference of the geometry cannot be recognized when *ka*<15.

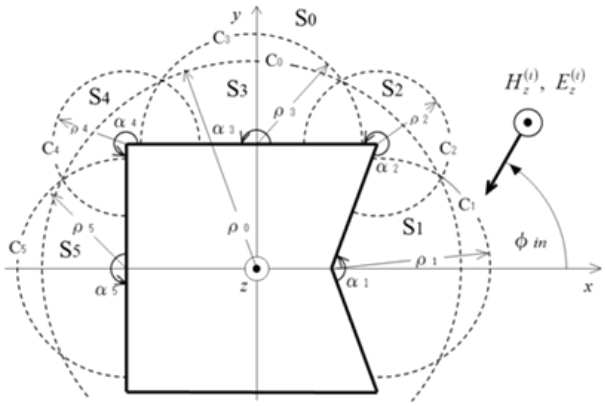


**Figure 1.** Field decomposition of PMM.

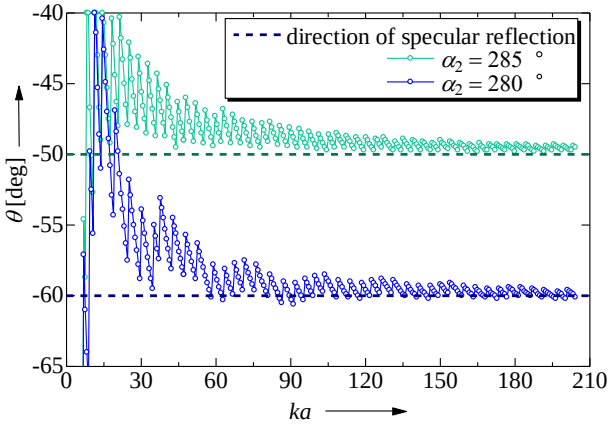


**Figure 2.** Peaks of the bistatic RCS for varying *ka*.

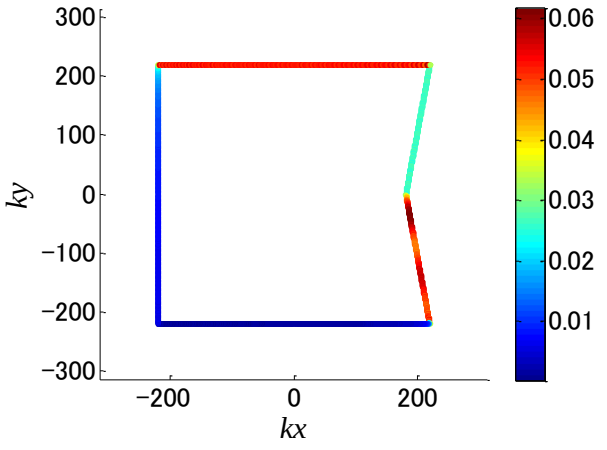


**Figure 3.** Surface current distribution for *ka* = 70π.

1: Graduate Course of Electrical Engineering, Graduate School of Science and Technology, Nihon University.
2:MITSUMI Electric Co.,Ltd. 3: Department of Electrical Engineering, College of Science and Technology, Nihon University

Figure 3 shows the surface current distribution $J = \left|\hat{\mathbf{n}} \times \overline{\mathbf{H}}^{(t)} / \overline{\mathbf{H}}^{(i)}\right|$ for $ka$ = 70π. The topside and underside of the cavity are illuminated regions where the current becomes large.

Figure 4 shows the surface current distribution for $ka$ = π. Compared with the result in Figure 3, the surface current on the upperside of the cavity becomes small.

Here, we consider the following radiation integral to clarify effects of the surface current on the upperside of the cavity;

$$\sigma(\theta) = \frac{k}{4}\left|\int_C J(x', y')\mathbf{n} \cdot \mathbf{R} \exp\left[jk(x'\cos\theta + y'\sin\theta)\right] dl'\right|^2 \quad (4)$$

Figure 5 shows the RCSs obtained by the PMM and the radiation integral which ignores the surface current on the upperside of the cavity. The two RCSs are almost equivalent at all the observation angles.

Figure 6 shows the RCSs for $ka$=π. They are different at almost all the observation angles. Compared with $ka$=70π, the contribution of the surface current on the upperside of the cavity is important.

Figure 7 shows the difference of the phase $\Delta\theta$ between similar geometries when $ka$=10π and 80π, such as

$$\Delta\theta_{(H_{z\_1} - H_{z\_2})} = \tan^{-1}\left(\frac{\mathrm{Re}\left[H_{z\_1}\right]}{\mathrm{Im}\left[H_{z\_1}\right]}\right) - \tan^{-1}\left(\frac{\mathrm{Re}\left[H_{z\_2}\right]}{\mathrm{Im}\left[H_{z\_2}\right]}\right) \quad (5)$$

where $H_{z\_1}$ indicates the magnetic field for $\alpha_2 = 275°$ and $H_{z\_2}$ indicates that for $\alpha_2 = 280°$. The difference of the phase can be clearly recognized around the reflection direction of the underside of the cavity. Compared with the case of $ka$=10π, the difference for $ka$=80π can be recognized in narrower area.

## 4. Conclusions

In this paper, we study electromagnetic scattering from polygonal conducting cylinders by using a kind of mode matching technique. Effects of slight variation of the geometry are clarified.

## 5. Acknowledgments

This work was partly supported by Nihon University Strategic Projects for Academic Research.

## 6. References

[1] S. Ohnuki, R. Ohsawa, and T. Yamasaki : "Electromagnetic Scattering from Rectangular Cylinders with Various Wedge Cavities and Bumps", *IEICE Trans. Electron.*, Vol.E93-C, No.1, pp.77-80, 2010.

[2] S. Ohnuki. S. Shinohara, R. Ohsawa, and T. Yamasaki : "Analysis of Electromagnetic Waves from Shadow Regions of Conducting Cylinders with Wedge Cavities", The 2011 International Symposium on Antennas and Propagation, Lotte Hotel Jeju, Jeju, Korea, Oct., 2011.

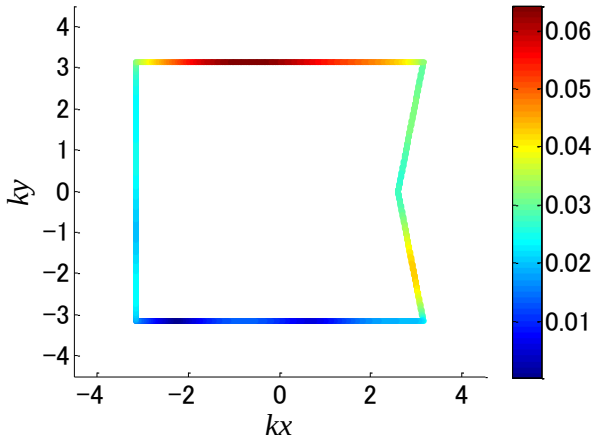


**Figure 4.** Surface current distribution for $ka$ = π.

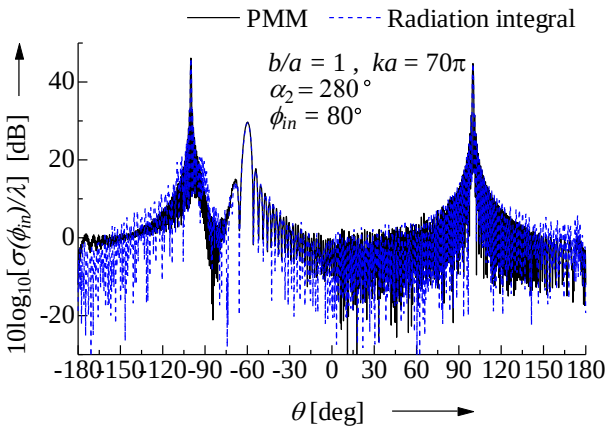


**Figure 5.** Bistatic RCS for $ka$ = 70π.

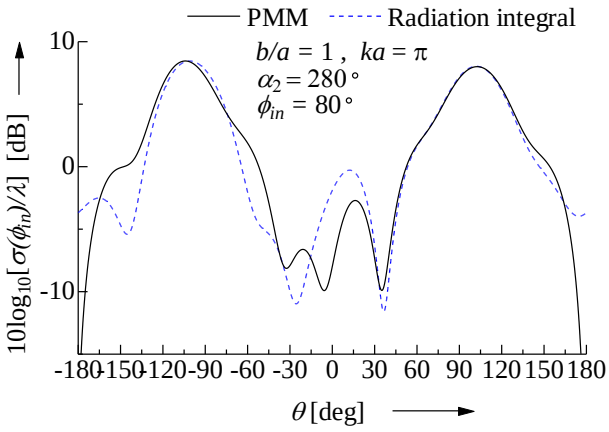


**Figure 6.** Bistatic RCS for $ka$ = π.

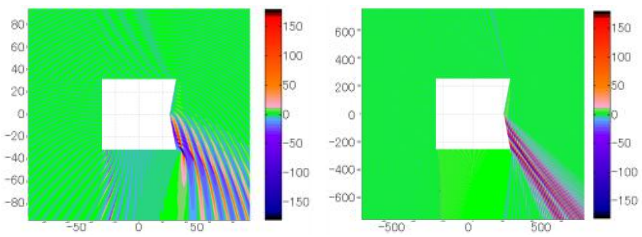

(a) $ka$=10π.　　(b) $ka$=80π.

**Figure 7.** Difference of phases for slight variation of the geometries.